Computational Mechanics (2019) 63:181–199
https://doi.org/10.1007/s00466-018-1590-9

ORIGINAL PAPER

A novel interface integral formulation for 3D steady state thermal conduction problem for a medium with non-homogenous inclusions

Y. P. Gong[1] · H. S. Yang[1] · C. Y. Dong[1]

Received: 22 January 2018 / Accepted: 1 June 2018 / Published online: 13 June 2018

Abstract

A novel regularized interface integral equation for three-dimensional steady state heat conduction problems with non-homogeneous inclusions is developed. The proposed formulation only contains the fundamental solution of isotropic matrix. As a result, the fundamental solution of non-homogeneous inclusion, usually very difficult to obtain, is avoided. Domain integrals caused by the contrast of heat conductivities between the inclusions and the matrix are converted into equivalent interface integrals using the radial integration method by expressing the temperature gradient as a series of radial basis functions. Therefore, a pure interface integral equation is obtained and there is no need to discretize the inclusion into finite elements to evaluate the domain integral. For the determination of the flux and temperature, collocation points are distributed inside the inclusion to form a system of linear equations. To eliminate the geometrical errors and study the inclusions with arbitrary geometry, bivariate Non-Uniform Rational B-Splines basis functions are used to depict the boundaries of the inclusions. Numerical results are compared with available analytical solutions or finite element solutions.

Keywords Heat conduction · Inclusion problems · Regularized interface integral equation · NURBS · Radial integration method

1 Introduction

The numerical computation of inclusion problems is of considerable technical importance, and significant progress in this field has been made since the pioneering work of Eshelby [1]. The methods used to study the inclusion problems usually include but are not limited to, complex function methods [2–4], finite element method [5–9], Green's functions method [10,11], finite difference method [11] and equivalent inclusion method [12]. Although great progresses have been achieved for each of the above methods, these methods exist some drawbacks, e.g. (1) some methods [2–4,10,11] are only suitable for some special problems with simple inclusion shapes; (2) some methods [5–9,12] need a finite element mesh discretization of the matrix and inclusions. Boundary element method (BEM) [13–20] has been proved to be an effective method in the analysis of inclusion problems, since it only requires the discretization of the model boundary into elements, rather than the whole body, thus being able to reduce the dimensionality of the problem by one. In [21–23], indirect boundary element method is used to study 2D elasticity problems, plane orthotropic elastic media and thermal stress analysis, respectively.

However, the BEM also faces a serious challenge when solving inclusion problems. One of the major problems is to adopt the fundamental solution of anisotropic medium which, in itself, is very complicated relative to isotropic medium when the BEM is used for the analysis of anisotropic inclusion problems, especially for 3D problems [24]. Furthermore, computation of domain integrals in the resulting integral equations will be time consuming [25–27]. To evaluate these domain integrals, the problem parts with domain integrals usually needs to be discretized into internal cells [27,28]. Although this integral method can give perfect results, the discretization of the domain into cells eliminates the distinct merit of the BEM in which only the boundary of the problem needs to be discretized into elements. Therefore, some scholars prefer to propose some schemes to transform domain integrals into boundary integrals rather than compute the domain integrals by the cell integration scheme.

✉ C. Y. Dong
cydong@bit.edu.cn

[1] Department of Mechanics, School of Aerospace Engineering, Beijing Institute of Technology, Beijing 100081, China

Up to now, tremendous effort has been devoted to transform domain integrals into boundary integrals and many extensively utilized transformation methods have been proposed, e.g. dual reciprocity method [29], multiple reciprocity method [30] and analytical integration method [31]. Both the dual reciprocity method and the multiple reciprocity method are powerful methods for domain integrals and widely used for practical problems. But the dual reciprocity method requires particular solutions, which may be very challenging to be obtained for some complicated basis functions. And for the numerical implementation of the multiple reciprocity method, a constant contained in the fundamental solutions should be defined which makes the results instable. The analytical integration method is only restricted to straight-line elements because it is hard to obtain analytical expression for curved line elements or surface elements. In 2002, an effective transformation method, called radial integration method, was developed by Gao [32] to tackle the elastoplastic problems. As shown in [20,32–35], for the domain integrals with unknown variables, the transformation will be accomplished with the use of the radial basis functions augmented by polynomials to approximate the unknown quantities as in the dual reciprocity method.

In 2005, a promising method called isogeometric analysis was established by Hughes et al. [36] as a way of bridging the gap between CAD and computer aided engineering (CAE). In the implementation of isogeometric analysis, geometries are usually represented by Non-Uniform Rational B-Splines (NURBS), which has been used in industrial CAD systems for decades due to the flexibility and precision for the representation of arbitrary geometry. The geometry described by NURBS can be enriched and refined easily by using the standard knot-insertion and/or degree-elevation procedures [36,37] without communicating with the CAD system, once the initial mesh is completed. This is an excellent property for interpolation of fields that requires high-order continuity, and leads to results with higher accuracy [38]. In [39], a material interface modeling has been discussed by isogeometric enriched quasi-convex meshfree method.

In addition, large scale problems are often encountered in engineering applications. In [40,41], the authors presented the 3D multiresolution theory and a stable micro-damage algorithm to solve some large-scale problems. Boundary element method is also powerful to solve large scale problem [42,43]. In this work, a novel interface-domain integral equation for large-scale 3D steady state heat conduction problems with non-homogeneous inclusions is developed. A similar derivation for steady-state elastoplastic problems can be found in [44]. Different from the traditional boundary element method for the analysis of anisotropic inclusion problems, only the fundamental solution of isotropic matrix is needed in the present formulation so that the fundamental solution of non-homogeneous inclusion is avoided. That is to say, the thermal conduction problem with non-homogeneous inclusions can be solved without computing the fundamental solution of anisotropic medium. The established interface-domain integral equation is regularized by using the add-subtraction technique. The domain integrals appearing in the regularized integral equation are converted into the equivalent interface integrals using the radial integration method by expressing the temperature gradient as a series of basis functions, which results in a pure interface integral equation and requires no internal cells to evaluate the domain integrals. In the numerical computation, the geometries of the inclusions are depicted by bivariate NURBS basis functions, which ensure the present method remarkable merit due to its integration of CAD, exact geometrical representation and high precision.

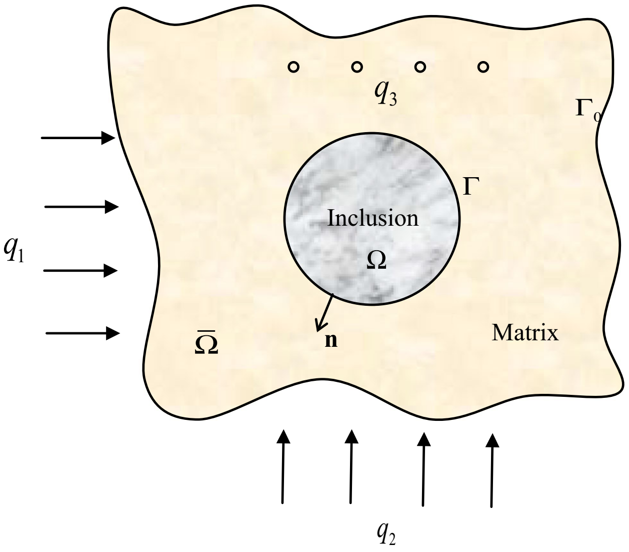

Fig. 1 Inclusion model

A brief outline of this paper is as follows. A regularized interface-domain integral equation for heat conduction problems with anisotropic inclusion is developed in Section 2. In Section 3, the domain integrals existing in the regularized integral equation are transformed into the equivalent interface integrals. Section 4 introduces isogeometric implementation of the regularized interface-domain integral equations. Several numerical examples are given in Section 5 to verify the accuracy of the present method. Finally, we present the conclusions for our work.

2 Regularized interface-domain integral equations for heat conduction problems

The inclusion problem considered in this paper is shown in Fig. 1. Let Ω be the inclusion domain made of material with heat conductivity k_{ij} embedded in the matrix ($\bar{\Omega}$) made of isotropic material with heat conductivity k. The perfectly bonded interface Γ between the inclusion and the matrix is assumed. Remote heat fluxes (q_1, q_2 and q_3) are applied to the matrix containing the inclusion of various shapes.

According to Fourier law [45], the heat fluxes t_i in Ω can be obtained by the following equation:

$$t_i = -k_{ij}\frac{\partial u}{\partial x_j} \tag{1}$$

where $i = 1, 2, 3$. x_j is the j-th component of the spatial coordinates at point $\mathbf{x}$ and u represents the temperature. The repeated subscript j represents the summation through its range which is 3 for 3D problems.

General material is assumed in the inclusion, so that the conductivity k_{ij} can be expressed as:

$$k_{ij} = k\delta_{ij} - \Delta k_{ij} \tag{2}$$

where δ_{ij} is the Kronecker delta symbol and Δk_{ij} denotes the contrast of heat conductivities between the inclusion and the matrix.

Using the principle of virtual work and Eq. (1), we have

$$\int_{\Omega} -k_{ij}\frac{\partial u}{\partial x_j}\frac{\partial U}{\partial x_i}d\Omega = \int_{\Gamma} t_i n_i U d\Gamma \tag{3}$$

where U is the virtual temperature, Γ is the interface between the domains Ω and $\bar{\Omega}$ as shown in Fig. 1, and n_i is the i-th component of outward normal vector $\mathbf{n}$ to the interface Γ.

Substituting Eq. (2) into Eq. (3) and according to Green formula, it follows that

$$\int_{\Gamma} T_j n_j u d\Gamma - \int_{\Omega} u\frac{\partial T_j}{\partial x_j}d\Omega + \int_{\Omega}\Delta k_{ij}\frac{\partial u}{\partial x_j}\frac{\partial U}{\partial x_i}d\Omega = \int_{\Gamma} tUd\Gamma \tag{4}$$

where $T_j = -k\delta_{ij}\frac{\partial U}{\partial x_i}$ and $t = t_i n_i$.

To derive the interface integral equation, the following equation is introduced to Eq. (4)

$$\frac{\partial T_j}{\partial x_j} + \delta(p, q) = 0 \tag{5}$$

where p and q are source point and field point, respectively. The Dirac delta function δ at point $p = q$ has an infinite value, but its integral gives unity, i.e.

$$\int_{\Omega}\delta(p, q)d\Omega = 1 \tag{6}$$

Hence, for any point $p \in \Omega$, the interface-domain integral equation can be expressed as

$$\begin{aligned} u(p) = &\int_{\Gamma} U(p, Q)t(Q)d\Gamma - \int_{\Gamma} T(p, Q)u(Q)d\Gamma \\ &- \int_{\Omega}\Delta k_{ij}(q)\frac{\partial U(p, q)}{\partial x_i(q)}\frac{\partial u(q)}{\partial x_j(q)}d\Omega \end{aligned} \tag{7}$$

where T is the virtual flux. In the present work, p represents the source point. q is the field point within the computational domain and Q is the field point on the boundary.

For the point $p \in \bar{\Omega}$, i.e. being outside the inclusion, the corresponding integral equation is of the following form:

$$\begin{aligned} &\int_{\Gamma} U^{-}(p, Q)t^{-}(Q)d\Gamma - \int_{\Gamma} T^{-}(p, Q)u^{-}(Q)d\Gamma \\ &+ \int_{\Gamma_0} U(p, Q)t(Q)d\Gamma - \int_{\Gamma_0} T(p, Q)u(Q)d\Gamma = 0 \end{aligned} \tag{8}$$

where Γ_0 is the outer boundary of matrix as shown in Fig. 1. The symbols with the superscript '$-$' in Eq. (8) represent the physical quantities being integrated along the inner boundary Γ of the matrix, whereas physical quantities without superscript in Eq. (8) will be integrated along the outer boundary Γ_0.

Along the interface Γ between the inclusion and matrix, the continuity condition requires that temperature calculated for the inclusion must equal the temperature calculated for the matrix. A similar relationship remains for the equilibrium condition along the interface between two domains, except that a negative sign must be given to account for the opposite directions of the outward boundary normal in the two domains. These conditions produce the following relationships along the interface of inclusion and matrix

$$\begin{aligned} &U(p, Q) = U^{-}(p, Q) \\ &T(p, Q) = -T^{-}(p, Q) \\ &u = u^{-} \\ &t = -t^{-} \end{aligned} \tag{9}$$

Adding Eq. (7) and Eq. (8), and using relationships in Eq. (9), one can obtain the following equation:

$$\begin{aligned} u(p) = &\int_{\Gamma_0} U(p, Q)t(Q)d\Gamma - \int_{\Gamma_0} T(p, Q)u(Q)d\Gamma \\ &- \int_{\Omega}\Delta k_{ij}(q)\frac{\partial U(p, q)}{\partial x_i(q)}\frac{\partial u(q)}{\partial x_j(q)}d\Omega \end{aligned} \tag{10}$$

In order to obtain the unknown quantities, the derivatives of Eq. (10) with respect to the coordinates x_k at the source point p give us the following integral equation:

$$\frac{\partial u(p)}{\partial x_k(p)} = \int_{\Gamma_0} \frac{\partial U(p,Q)}{\partial x_k(p)} t(Q) d\Gamma - \int_{\Gamma_0} \frac{\partial T(p,Q)}{\partial x_k(p)} u(Q) d\Gamma - \int_{\Omega} \Delta k_{ij}(q) \frac{\partial^2 U(p,q)}{\partial x_i(q) \partial x_k(p)} \frac{\partial u(q)}{\partial x_j(q)} d\Omega \tag{11}$$

where $k = 1, 2, 3$. $U(p, Q)$ and $T(p, Q)$ represent the fundamental solutions expressed as:

$$U(p,Q) = \frac{1}{4\pi r k} \tag{12}$$

and

$$T(p,Q) = -k\frac{\partial U}{\partial \mathbf{n}} = \frac{1}{4\pi r^2}\frac{\partial r}{\partial \mathbf{n}} \tag{13}$$

where r denotes the distance between the source and the field points. Now, the unknowns u and $\frac{\partial u}{\partial x_j}$ can be obtained by solving system of equations constructed by Eqs. (10) and (11).

In practical engineering problems, the size of inclusion is often relatively small compared to the dimension of matrix. Therefore, the infinite problems ($\Gamma_0 \to \infty$) tend to attract more attention from engineers. In this paper, we focus our attention on the computation of the infinite problems. For an infinite isotropic matrix containing one inclusion, the above Eqs. (10) and (11) can be simplified as

$$u(p) = u^0(p) - \int_{\Omega} \Delta k_{ij}(q) \frac{\partial U(p,q)}{\partial x_i(q)} \frac{\partial u(q)}{\partial x_j(q)} d\Omega \tag{14}$$

$$\frac{\partial u(p)}{\partial x_k(p)} = \frac{\partial u^0(p)}{\partial x_k(p)} - \int_{\Omega} \Delta k_{ij}(q) \frac{\partial^2 U(p,q)}{\partial x_i(q)\partial x_k(p)} \frac{\partial u(q)}{\partial x_j(q)} d\Omega \tag{15}$$

where u^0 and $\frac{\partial u^0}{\partial x_k}$ represent temperature and gradient at collocation point $p \in \Omega$ due to the remote heat flux in the matrix not containing inclusions.

Eqs. (14) and (15) are the domain integral equations for the steady state heat conduction problems with non-homogeneous inclusion embedded in an infinite matrix. In contrast to the conventional BEM formulations, Eqs. (14) and (15) include domain integrals. Clearly, the domain integrals are singular when the source point is located in the inclusion domain Ω. In this paper, we will use the add-subtraction technique to regularize the singularity involved in kernels.

Take the domain integral in Eq. (14) as an example. Extracting the singular term in the integral representation of temperature gradients, we obtain regularized integral representation of the singular domain integral

$$\begin{aligned}
&\int_{\Omega} \Delta k_{ij}(q) \frac{\partial U(p,q)}{\partial x_i(q)} \frac{\partial u(q)}{\partial x_j(q)} d\Omega \\
&= \int_{\Omega} \frac{\partial U(p,q)}{\partial x_i(q)} \left(\Delta k_{ij}(q) \frac{\partial u(q)}{\partial x_j(q)} - \Delta k_{ij}(p) \frac{\partial u(p)}{\partial x_j(p)} \right) d\Omega \\
&\quad + \int_{\Omega} \Delta k_{ij}(p) \frac{\partial u(p)}{\partial x_j(p)} \frac{\partial U(p,q)}{\partial x_i(q)} d\Omega \\
&= \int_{\Omega} \frac{\partial U(p,q)}{\partial x_i(q)} \left(\Delta k_{ij}(q) \frac{\partial u(q)}{\partial x_j(q)} - \Delta k_{ij}(p) \frac{\partial u(p)}{\partial x_j(p)} \right) d\Omega \\
&\quad + \Delta k_{ij}(p) \frac{\partial u(p)}{\partial x_j(p)} \int_{\Gamma_\Omega} U(p,Q) n_i d\Gamma
\end{aligned} \tag{16}$$

where Γ_Ω is the boundary of domain Ω.

And similar procedure can be repeated also for the domain integral in Eq. (15), i.e.

$$\begin{aligned}
&\int_{\Omega} \Delta k_{ij}(q) \frac{\partial^2 U(p,q)}{\partial x_i(q)\partial x_k(p)} \frac{\partial u(q)}{\partial x_j(q)} d\Omega \\
&= \int_{\Omega} \frac{\partial^2 U(p,q)}{\partial x_i(q)\partial x_k(p)} \left(\Delta k_{ij}(q) \frac{\partial u(q)}{\partial x_j(q)} - \Delta k_{ij}(p) \frac{\partial u(p)}{\partial x_j(p)} \right) d\Omega \\
&\quad + \Delta k_{ij}(p) \frac{\partial u(p)}{\partial x_j(p)} \int_{\Gamma_\Omega} U(p,Q) n_i d\Gamma
\end{aligned} \tag{17}$$

Therefore, substituting Eqs. (16) and (17) into Eqs. (14) and (15), respectively, we obtain the regularized integral representation of temperature and gradient

$$\begin{aligned}
u(p) = u^0(p) &- \int_{\Omega} \frac{\partial U(p,q)}{\partial x_i(q)} \\
&\times \left(\Delta k_{ij}(q) \frac{\partial u(q)}{\partial x_j(q)} - \Delta k_{ij}(p) \frac{\partial u(p)}{\partial x_j(p)} \right) d\Omega \\
&- \Delta k_{ij}(p) \frac{\partial u(p)}{\partial x_j(p)} \int_{\Gamma_\Omega} U(p,Q) n_i d\Gamma
\end{aligned} \tag{18}$$

and

$$\begin{aligned}
\frac{\partial u(p)}{\partial x_k(p)} = \frac{\partial u^0(p)}{\partial x_k(p)} &- \int_{\Omega} \frac{\partial^2 U(p,q)}{\partial x_i(q)\partial x_k(p)} \left(\Delta k_{ij}(q) \frac{\partial u(q)}{\partial x_j(q)} \right. \\
&\left. - \Delta k_{ij}(p) \frac{\partial u(p)}{\partial x_j(p)} \right) d\Omega \\
&- \Delta k_{ij}(p) \frac{\partial u(p)}{\partial x_j(p)} \int_{\Gamma_\Omega} U(p,Q) n_i d\Gamma
\end{aligned} \tag{19}$$

For multiple inclusions (Ω^i, $i = 1, 2, \cdots, \mathrm{NI}$, NI is the number of inclusions) as shown in Fig. 2, the extensions of Eqs. (18–19) are as follows:

$$\begin{aligned}
u(p) = u^0(p) &- \Delta k_{ij}^b(p) \frac{\partial u(p)}{\partial x_j(p)} \int_{\Gamma_{\Omega^b}} U(p,Q) n_i d\Gamma \\
&- \int_{\Omega^b} \frac{\partial U(p,q)}{\partial x_i(q)} \left(\Delta k_{ij}^b(q) \frac{\partial u(q)}{\partial x_j(q)} - \Delta k_{ij}^b(p) \frac{\partial u(p)}{\partial x_j(p)} \right) d\Omega \\
&- \sum_{s=1,\neq b}^{\mathrm{NI}} \int_{\Omega^s} \Delta k_{ij}^s(q) \frac{\partial U(p,q)}{\partial x_i(q)} \frac{\partial u(q)}{\partial x_j(q)} d\Omega
\end{aligned} \tag{20}$$

$$\frac{\partial u(p)}{\partial x_k(p)} = \frac{\partial u^0(p)}{\partial x_k(p)} - \Delta k_{ij}^b(p) \frac{\partial u(p)}{\partial x_j(p)} \int_{\Gamma_{\Omega^b}} U(p,Q) n_i d\Gamma$$

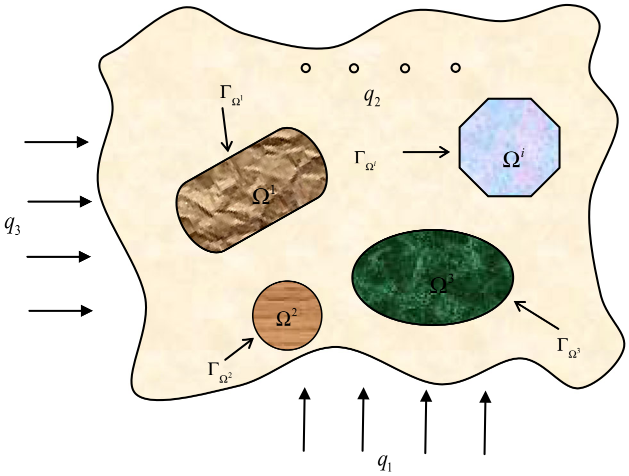

Fig. 2 Multiple inclusions model

$$-\int_{\Omega^b}\frac{\partial^2 U(p,q)}{\partial x_i(q)\partial x_k(p)}\left(\Delta k_{ij}^b(q)\frac{\partial u(q)}{\partial x_j(q)}-\Delta k_{ij}^b(p)\frac{\partial u(p)}{\partial x_j(p)}\right)d\Omega$$
$$-\sum_{s=1,\neq b}^{\mathrm{NI}}\int_{\Omega^s}\Delta k_{ij}^s(q)\frac{\partial^2 U(p,q)}{\partial x_i(q)\partial x_k(p)}\frac{\partial u(q)}{\partial x_j(q)}d\Omega \tag{21}$$

where Ω^b denotes the b-th inclusion with boundary Γ_{Ω^b} and contains source point p as an interior point. $\Delta k_{ij}^s(\Delta k_{ij}^b)$ is the contrast of heat conductivities between the s-th (b-th) inclusion and the matrix

3 Transformation of domain integral to the interface integral

In this section, the two domain integrals involved in Eqs. (20) and (21) are transformed into equivalent interface integrals by using the radial integration method. Since the domain integrals of Eqs. (20) and (21) contain unknown gradient $\partial u/\partial x_j$, the volume integrals cannot be transformed into contour integrals directly. To solve this problem, the method proposed by Gao [32] is adopted. The unknown gradient $\partial u/\partial x_j$ is expressed as a combination of radial basis functions and polynomials in global coordinates, i.e.

$$\frac{\partial u(q)}{\partial x_j(q)}=\sum_{A=1}^{N}a_j^A\phi_j^A(R)+C_j^0+\sum_{\mu=1}^{m}C_j^\mu x_\mu \tag{22}$$

and

$$\sum_{A=1}^{N}a_j^A=\sum_{A=1}^{N}a_j^A x_\mu^A=0$$

where N is the number of the given collocation points in all the inclusions. a_j^A, C_j^0, and C_j^μ represent coefficients to be determined. x_μ^A is the μ-th coordinate component at the application point A. m indicates the dimension of the considered problems (2 for 2D and 3 for 3D). ϕ_j^A is the radial basis function. In Eq. (22), the number of terms required in the computation depends on the character of the computed model, such as the boundary geometry of the model, properties of inclusions and the heat flux in the domain.

Substituting Eq. (22) into Eqs. (20) and (21), the domain integrals can be transformed into contour integrals, for example

$$\begin{aligned}&\int_{\Omega^b}\frac{\partial^2 U(p,q)}{\partial x_i(q)\partial x_k(p)}\left(\Delta k_{ij}^b(q)\frac{\partial u(q)}{\partial x_j(q)}-\Delta k_{ij}^b(p)\frac{\partial u(p)}{\partial x_j(p)}\right)d\Omega\\&=\alpha_j^A\int_{\Gamma^b}\frac{1}{r^\beta(Q,p)}\frac{\partial r}{\partial \mathbf{n}}F_j^A(Q,p)d\Gamma\\&\quad+C_j^0\int_{\Gamma^b}\frac{1}{r^\beta(Q,p)}\frac{\partial r}{\partial \mathbf{n}}F_j^0(Q,p)d\Gamma\\&\quad+C_j^\mu\int_{\Gamma^b}\frac{1}{r^\beta(Q,p)}\frac{\partial r}{\partial \mathbf{n}}F_j^\mu(Q,p)d\Gamma\end{aligned} \tag{23}$$

where $r(Q,p)$ is the distance between the field point Q (on the interface Γ^b) and the source point p, and

$$\begin{aligned}F_j^A(Q,p)&=\int_0^r\frac{\partial^2 U(p,q)}{\partial x_i(q)\partial x_k(p)}\Big(\Delta k_{ij}^b(q)\phi_j^A(R)\\&\qquad-\Delta k_{ij}^b(p)\phi_j^A(R)\Big)\,r^\beta dr\\F_j^0(Q,p)&=\int_0^r\frac{\partial^2 U(p,q)}{\partial x_i(q)\partial x_k(p)}r^\beta dr\\F_j^\mu(Q,p)&=\int_0^r\frac{\partial^2 U(p,q)}{\partial x_i(q)\partial x_k(p)}(x_\mu(q)-x_\mu(p))r^\beta dr\end{aligned} \tag{24}$$

It is noted that since r^β ($\beta=1$for 2D and $\beta=2$ for 3D) is included in Eq. (24), there are no singularity problems in Eqs. (23) and (24). Therefore, the integrals can be evaluated numerically using Gaussian quadrature method. It should be pointed out that the distance R used in the Eq. (24) is from the application point A to the field point q, but the distance r existing in the fundamental solutions of Eqs. (23) and (24) is from the source point p to the field point q. Figure 3a, b gives some illustration for their relations.

To our knowledge, the case when the computed point p is inside the domain (Fig. 3a) has been studied and applied to investigate practical problems [32–35]. Here we will pay more attention on the case when the computed point is outside of the domain, which will be important for us to calculate the physical quantities of points in the matrix. As shown in Fig. 3b, a point $\bar{p}$ in the domain is defined to transform the domain integral to the boundary integral. The reference point $\bar{p}$ is used to obtain the field point (q) along radial direction. From Fig. 3b, we can see that vector $\vec{r}=\overrightarrow{p\bar{p}}+\overrightarrow{\bar{p}q}$ ($\bar{p}$ can be any point in the domain). When the computed point is inside

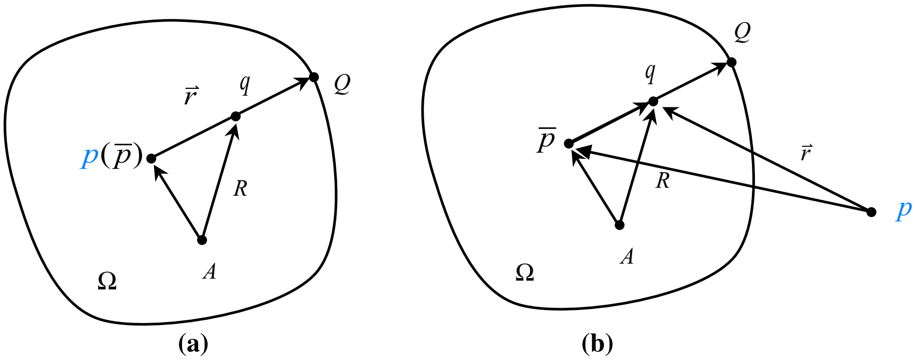

Fig. 3 Relationship among source point p, field point q, application point A and distances R and r. **a** Source point is within the domain, **b** source point is outside the domain

the domain (Fig. 3a), we usually make the computed point $p = \bar{p}$. That is to say, Fig. 3b is a general case of Fig. 3a (p and $\bar{p}$ are the same points in Fig. 3a).

Following the method above, all the volume integrals appearing in the regularized interface-domain integral equation (Eqs. 20, 21) can be converted to the interface integrals. Then, a strictly regularized interface integral equation is formed, and only the interface between the inclusion and matrix needs to be discretized into boundary elements as shown in Eqs. (23) and (24). The resulting system of equations containing unknown coefficients of Eq. (22) can be formed through a collocation procedure. Once these coefficients are determined, the temperature and flux at general points in the matrix and inclusions can be obtained.

4 Isogeometric implementation of the regularized interface integral equations

In this work, the isogeometric boundary element method is adopted to study the present problems, that is, the NURBS basis functions are used to describe the geometry of the problem and to approximate physical quantities appearing in the regularized interface integral equations for steady state heat conduction problems. For completeness, the simple introduction about NURBS bases is shown below, whereas more details about the isogeometric boundary element method can be found in [36,46–50].

NURBS bases are built up from B-splines, which are defined recursively with piecewise constants. A B-spline basis ($N_{i,p}$) of degree p is generated based on knot vector $\mathbf{U}$ $\{= \xi_1, \xi_2, \ldots, \xi_{n+p+1}\}$, where $\xi_1 \leq \xi_2 \leq \cdots \leq \xi_{n+p+1}$, each $\xi_i \in R$ is a knot, and n is the associated number of control points. Then the basis functions are denoted by $N_{i,p}$ with $1 \leq i \leq n$ and are defined as follows [36]:

for $p = 0$

$$N_{i,0} = \begin{cases} 1 \text{ if } \xi_i \leq \xi < \xi_{i+1}, \\ 0 \text{ otherwise.} \end{cases} \tag{25}$$

and for $p = 1, 2, 3, \cdots$:

$$N_{i,p} = \frac{\xi - \xi_i}{\xi_{i+p} - \xi_i} N_{i,p-1}(\xi) + \frac{\xi_{i+p+1} - \xi}{\xi_{i+p+1} - \xi_{i+1}} N_{i+1,p-1}(\xi) \tag{26}$$

For NURBS bases $R_{i,p}(\xi)$, a weight ω_i is assigned to every B-spline function $N_{i,p}(\xi)$. And NURBS basis functions are defined as [36]

$$R_{i,p}(\xi) = \frac{N_{i,p}(\xi)\omega_i}{\sum_{j=1}^{n} N_{j,p}(\xi)\omega_j} \tag{27}$$

NURBS surface can be represented as follows [36]:

$$S(\xi, \eta) = \sum_{i=1}^{n} \sum_{j=1}^{m} R_{i,j}^{p,q}(\xi, \eta) P_{i,j} \tag{28}$$

where $S(\xi, \eta)$ is the vector with Cartesian coordinates of the point described by the parametric point $\xi_1 \leq \xi \leq \xi_{n+p+1}$ and $\eta_1 \leq \eta \leq \eta_{m+q+1}$. The bivariate basis functions $R_{i,j}^{p,q}$ are given by

$$R_{i,j}^{p,q}(\xi, \eta) = \frac{N_i(\xi) M_j(\eta) \omega_{i,j}}{\sum_{\hat{i}=1}^{n} \sum_{\hat{j}=1}^{m} N_{\hat{i}}(\xi) M_{\hat{j}}(\eta) \omega_{\hat{i},\hat{j}}} \tag{29}$$

where $N_{i,p}$ is the ith B-spline basis function of order p and $M_{j,q}$ is the jth B-spline basis function of order q. $\omega_{i,j}$ is the weight corresponding to the control point $P_{i,j}$.

In the present work, the isogeometric analysis relies on the use of the bivariate NURBS basis functions given above. In the implementation of computation, two knot vectors $\mathbf{U}$ and $\mathbf{V}$, $m \times n$ control points $P_{i,j}$ and curve orders p and q are used to build the boundary shape and the basis functions. Isogeometric elements of the integral boundary are defined in the parametric space as non-zero knots span $[\xi_i,\ \xi_{i+1}] \times [\eta_j,\ \eta_{j+1}]$, where $\xi_i,\ \xi_{i+1} \in \mathbf{U}$ and $\eta_j,\ \eta_{j+1} \in \mathbf{V}$. In this paper, Gauss–Legendre quadrature is used for the nonsingular integrals. Therefore, a transformation from the parameter space $(\xi, \eta) \in \left[\xi_i,\ \xi_{i+1}\right] \times \left[\eta_j,\ \eta_{j+1}\right]$ to the Gauss–Legendre range $[-1,\ 1]\times[-1,\ 1]$ should be adopted. The Jacobian of transformation from the physical domain to a parametric domain is given by [45]

$$\left|J_{(\xi,\eta)}\right| = \left[\left(\frac{\partial x_2}{\partial \xi}\frac{\partial x_3}{\partial \eta} - \frac{\partial x_3}{\partial \xi}\frac{\partial x_2}{\partial \eta}\right)^2 + \left(\frac{\partial x_3}{\partial \xi}\frac{\partial x_1}{\partial \eta} - \frac{\partial x_1}{\partial \xi}\frac{\partial x_3}{\partial \eta}\right)^2 + \left(\frac{\partial x_1}{\partial \xi}\frac{\partial x_2}{\partial \eta} - \frac{\partial x_2}{\partial \xi}\frac{\partial x_1}{\partial \eta}\right)^2\right]^{1/2} \tag{30}$$

and Jacobian of the transformation from the parent domain to a parametric domain reads [50]

$$\left|J_{(\bar{\xi},\bar{\eta})}\right| = \frac{1}{4}\left(\xi_{i+1} - \xi_i\right)\left(\eta_{j+1} - \eta_j\right) \tag{31}$$

Local basis functions that are related to the global basis functions are defined as [46,50]

$$N_l^e(\bar{\xi}, \bar{\eta}) \equiv R_a^{p,q}(\xi(\bar{\xi}), \eta(\bar{\eta})) \tag{32}$$

where the local basis function number l, element number e and global basis function number are related by $a = \mathrm{conn}(e, l)$, where conn() is a connectivity function. The geometry of the problem can be easily interpolated as

$$\mathbf{x}_e(\bar{\xi}, \bar{\eta}) = \sum_{l=1}^{(p+1)(q+1)} N_l^e(\bar{\xi}, \bar{\eta})\mathbf{x}_l \tag{33}$$

where $\mathbf{x}_l$ represents the coordinate at a particular control point.

Then, we can obtain the isogeometric boundary integral equations for Eqs. (20) and (21) as follows

$$\begin{aligned}
u(p) = {} & u^0(p) - \Delta k_{ij}^b(p)\frac{\partial u(p)}{\partial x_j(p)}\sum_{e=1}^{N\Gamma_b} \sum_{l=1}^{(p+1)(q+1)} \int_{-1}^{1}\int_{-1}^{1} U(p, Q)n_i J(\bar{\xi}, \bar{\eta})d\bar{\xi}d\bar{\eta} \\
& - \left(\alpha_j^{A_b}\sum_{e=1}^{N\Gamma_b}\sum_{l=1}^{(p+1)(q+1)}\int_{-1}^{1}\int_{-1}^{1}\frac{1}{r^\beta(Q,p)}\frac{\partial r}{\partial \mathbf{n}} F_j^{A_b}(Q,p)J(\bar{\xi},\bar{\eta})d\bar{\xi}d\bar{\eta}\right. \\
& + C_j^{0_b}\sum_{e=1}^{N\Gamma_b}\sum_{l=1}^{(p+1)(q+1)}\int_{-1}^{1}\int_{-1}^{1}\frac{1}{r^\beta(Q,p)}\frac{\partial r}{\partial \mathbf{n}} F_j^{0_b}(Q,p)J(\bar{\xi},\bar{\eta})d\bar{\xi}d\bar{\eta} \\
& \left. + C_j^{\mu_b}\sum_{e=1}^{N\Gamma_b}\sum_{l=1}^{(p+1)(q+1)}\int_{-1}^{1}\int_{-1}^{1}\frac{1}{r^\beta(Q,p)}\frac{\partial r}{\partial \mathbf{n}} F_j^{\mu_b}(Q,p)J(\bar{\xi},\bar{\eta})d\bar{\xi}d\bar{\eta}\right) \\
& - \sum_{s=1,\neq b}^{\mathrm{NI}}\left(\alpha_j^{A_s}\sum_{e=1}^{N\Gamma_s}\sum_{l=1}^{(p+1)(q+1)}\int_{-1}^{1}\int_{-1}^{1}\frac{1}{r^\beta(Q,p)}\frac{\partial r}{\partial \mathbf{n}} F_j^{A_s}(Q,p)J(\bar{\xi},\bar{\eta})d\bar{\xi}d\bar{\eta}\right. \\
& + C_j^{0_s}\sum_{e=1}^{N\Gamma_s}\sum_{l=1}^{(p+1)(q+1)}\int_{-1}^{1}\int_{-1}^{1}\frac{1}{r^\beta(Q,p)}\frac{\partial r}{\partial \mathbf{n}} F_j^{0_s}(Q,p)J(\bar{\xi},\bar{\eta})d\bar{\xi}d\bar{\eta} \\
& \left. + C_j^{\mu_s}\sum_{e=1}^{N\Gamma_s}\sum_{l=1}^{(p+1)(q+1)}\int_{-1}^{1}\int_{-1}^{1}\frac{1}{r^\beta(Q,p)}\frac{\partial r}{\partial \mathbf{n}} F_j^{\mu_s}(Q,p)J(\bar{\xi},\bar{\eta})d\bar{\xi}d\bar{\eta}\right)
\end{aligned} \tag{34}$$

and

$$\begin{aligned}
\frac{\partial u(p)}{\partial x_k(p)} = {} & \frac{\partial u^0(p)}{\partial x_k(p)} - \Delta k_{ij}^b(p)\frac{\partial u(p)}{\partial x_j(p)}\sum_{e=1}^{N\Gamma_b} \sum_{l=1}^{(p+1)(q+1)} \int_{-1}^{1}\int_{-1}^{1} U(p, Q)n_i J(\bar{\xi}, \bar{\eta})d\bar{\xi}d\bar{\eta} \\
& - \left(\alpha_j^{A_b}\sum_{e=1}^{N\Gamma_b}\sum_{l=1}^{(p+1)(q+1)}\int_{-1}^{1}\int_{-1}^{1}\frac{1}{r^\beta(Q,p)}\frac{\partial r}{\partial \mathbf{n}} F_j^{A_b}(Q,p)J(\bar{\xi},\bar{\eta})d\bar{\xi}d\bar{\eta}\right. \\
& + C_j^{0_b}\sum_{e=1}^{N\Gamma_b}\sum_{l=1}^{(p+1)(q+1)}\int_{-1}^{1}\int_{-1}^{1}\frac{1}{r^\beta(Q,p)}\frac{\partial r}{\partial \mathbf{n}} F_j^{0_b}(Q,p)J(\bar{\xi},\bar{\eta})d\bar{\xi}d\bar{\eta} \\
& \left. + C_j^{\mu_b}\sum_{e=1}^{N\Gamma_b}\sum_{l=1}^{(p+1)(q+1)}\int_{-1}^{1}\int_{-1}^{1}\frac{1}{r^\beta(Q,p)}\frac{\partial r}{\partial \mathbf{n}} F_j^{\mu_b}(Q,p)J(\bar{\xi},\bar{\eta})d\bar{\xi}d\bar{\eta}\right) \\
& - \sum_{s=1,\neq b}^{\mathrm{NI}}\left(\alpha_j^{A_s}\sum_{e=1}^{N\Gamma_s}\sum_{l=1}^{(p+1)(q+1)}\int_{-1}^{1}\int_{-1}^{1}\frac{1}{r^\beta(Q,p)}\frac{\partial r}{\partial \mathbf{n}} F_j^{A_s}(Q,p)J(\bar{\xi},\bar{\eta})d\bar{\xi}d\bar{\eta}\right. \\
& + C_j^{0_s}\sum_{e=1}^{N\Gamma_s}\sum_{l=1}^{(p+1)(q+1)}\int_{-1}^{1}\int_{-1}^{1}\frac{1}{r^\beta(Q,p)}\frac{\partial r}{\partial \mathbf{n}} F_j^{0_s}(Q,p)J(\bar{\xi},\bar{\eta})d\bar{\xi}d\bar{\eta} \\
& \left. + C_j^{\mu_s}\sum_{e=1}^{N\Gamma_s}\sum_{l=1}^{(p+1)(q+1)}\int_{-1}^{1}\int_{-1}^{1}\frac{1}{r^\beta(Q,p)}\frac{\partial r}{\partial \mathbf{n}} F_j^{\mu_s}(Q,p)J(\bar{\xi},\bar{\eta})d\bar{\xi}d\bar{\eta}\right)
\end{aligned} \tag{35}$$

where $J(\bar{\xi},\bar{\eta}) = J_{(\xi,\eta)} \cdot J_{(\bar{\xi},\bar{\eta})}$. $N\Gamma_b(N\Gamma_s)$ is the total boundary elements for the b-th (s-th) inclusion. $\frac{\partial u(p)}{\partial x_j(p)}$ and $\frac{\partial u(p)}{\partial x_k(p)}$ can be computed by Eq. (22) for the case $p = q$. $F_j^{A_g}(Q, p)$, $F_j^{0_g}(Q, p)$ and $F_j^{\mu_g}(Q, p)$ ($g = b$ or s) are the radial integrals for the g-th inclusion as shown in Eq. (24). It should be noted that the kernels of radial integrals ($F_j^{A_g}(Q, p)$, $F_j^{0_g}(Q, p)$ and $F_j^{\mu_g}(Q, p)$) for Eqs. (34) and (35) are different. $\alpha_j^{A_g}$, $C_j^{0_g}$ and $C_j^{\mu_g}$ are the coefficients need to be computed in Eq. (23) for the g-th inclusion. $u^0(p)$ and $\frac{\partial u^0}{\partial x_k}$ are the temperature and gradient at collocation point $p \in \Omega$ due to the remote heat flux in the matrix not containing inclusions. For Eqs. (34) and (35), we use the Gauss-Legendre quadrature to deal with the regular boundary integrals. And both the strongly and weakly singular integrals are computed by the power series expansion method.

5 Results and discussions

Through several numerical examples, the accuracy and effectiveness of the present method for the three-dimensional heat transfer problems with inclusions are demonstrated in this section. In all the examples, we compare our results with those obtained by the analytical method or the FEM (Abaqus). The geometry of the inclusion is described by bivariate NURBS basis functions. In this paper, the isogeometric models of inclusions are built by Rhinoceros 5.0, and the following radial basis function is used

$$\sqrt{R^2+1} \tag{36}$$

where R is the distance from the application point to the field point as shown in Fig. 3a, b.

As introduced above, collocation points play an important role in the present method. Here, we will give the collocation procedure for the radial basis function method. Collocation points inside the spherical inclusions studied in examples 5.1-5.3 can be obtained by the following parameter equations:

$$\begin{aligned} x_1 &= (k \cdot \Delta L_1)\cos\theta_i \sin\phi_j \\ x_2 &= (k \cdot \Delta L_2)\sin\theta_i \sin\phi_j \\ x_3 &= (k \cdot \Delta L_3)\cos\phi_j \end{aligned} \tag{37}$$

where $\Delta L_1 = \Delta L_2 = \Delta L_3 = a/L$ for spherical inclusion. a is the radius of the inclusion and L ($= 4$) is an integer. k is an integer associated with L and $0 < k \le L - 1$. θ_i and ϕ_j are the i-th and j-th values of θ and ϕ, respectively, i.e.

$$\theta = \{\pi/4, 3\pi/4, 5\pi/4, 7\pi/4\}, \quad \phi = \{\pi/4, 3\pi/4\} \tag{38}$$

Similarly, collocations for prolate spherical inclusion investigated in example 5.4 can be obtained according to Eqs. (37) and (38) with $\Delta L_1 = a/L$, $\Delta L_2 = b/L$ and $\Delta L_3 = c/L$, where a, b, c are semi-axes.

The collocations of the two prolate spherical inclusions investigated in example 5.5 will be computed by the following parameter equations. For the right inclusion,

$$\begin{cases} x_1 = (k \cdot \Delta L_1)\cos\theta_i \sin\phi_j \\ x_2 = (k \cdot \Delta L_2)\sin\theta_i \sin\phi_j + 1.5 \\ x_3 = (k \cdot \Delta L_3)\cos\phi_j \end{cases} \tag{39}$$

and the left inclusion

$$\begin{cases} x_1 = (k \cdot \Delta L_1)\cos\theta_i \sin\phi_j \\ x_2 = (k \cdot \Delta L_2)\sin\theta_i \sin\phi_j - 1.5 \\ x_3 = (k \cdot \Delta L_3)\cos\phi_j \end{cases} \tag{40}$$

The values of parameters in Eqs. (39) and (40) are the same as above.

5.1 A single spherical inclusion embedded in an infinite matrix for the case $k_I < k_M$

As shown in Fig. 4, a single spherical air void ($0 \le r < a$, $a = 1$) embedded in an infinite isotropic borosilicate glass is investigated. The temperature T tends to $x_3 \cdot q_3/k_M$ at great distances. The heat conductivities of the inclusion (air) and matrix (borosilicate glass) are taken as $k_I = 0.03$ W/m K [51] and $k_M = 1.13$ W/m K[52], respectively. Here, a constant heat flux field along x_3 axis negative direction ($q_3 = 1.13$ W/m^2) is applied on the matrix, such that a steady-state heat flux field is produced but the local heat flux field is disturbed by the material mismatch between the inclusion and the matrix.

The corresponding polynomial orders and knot vectors are given in Table 1 and the control points, which can be obtained

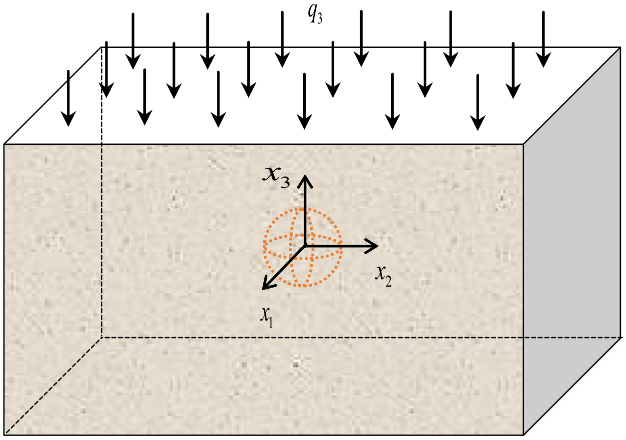

Fig. 4 The model of matrix and inclusion

Table 1 Polynomial orders and knot vectors for the inclusion

Direction	Order	Knot vector
ξ	$p = 2$	$\mathbf{U} = \{0,0,0,1,1,2,2,3,3,4,4,4\}$
η	$q = 2$	$\mathbf{V} = \{0,0,0,1,1,1\}$

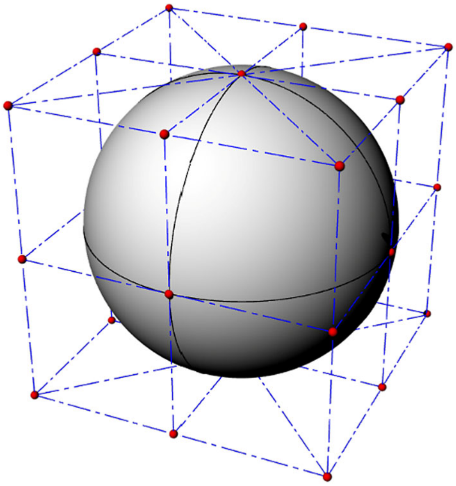

Fig. 5 Isogeometric model of the inclusion and its control points

from Rhinoceros, are given in Fig. 5. ξ and η correspond to two parametric directions in parameter space, respectively.

Based on the results in [53], the analytical solutions of gradient for this problem inside the inclusion can be obtained as:

$$\frac{\partial T}{\partial x_3} = \frac{3k_M}{2k_M + k_I} \tag{41}$$

and the exact results of gradient outside the inclusion are

$$\frac{\partial T}{\partial x_3} = 1 + \frac{a^3(k_M - k_I)}{r^3(2k_M + k_I)}(1 - 3\cos^2\theta) \tag{42}$$

where r and θ are spherical polar coordinates.

Figure 6 compares the heat flux distribution along the x_2 and x_3 for the present results and analytical solutions. It is interesting to note that along the axis x_2, the magnitude of heat flux field keeps nearly 1.13 W/m^2 far away from the inclusion, but highly discontinuous across the interface. The heat flux reaches a peak at the outer surface of the inclusion and then gradually decreases to q_3 in the far field of the matrix material. Different from the values in Fig. 6a, along the axis x_3, there is no jumping for the distribution of heat flux field near the inclusion domain. And the distribution of heat flux field is continuous even across the interface. As shown in Fig. 6b, the heat flux is also convergent to 1.13 W/m^2, which is the far field constant loading q_3. From Fig. 6a, b, we can see that the present results are in excellent agreement with the analytical solutions. For this problem, similar conclusion as [51] can be obtained: the heat flux field is almost

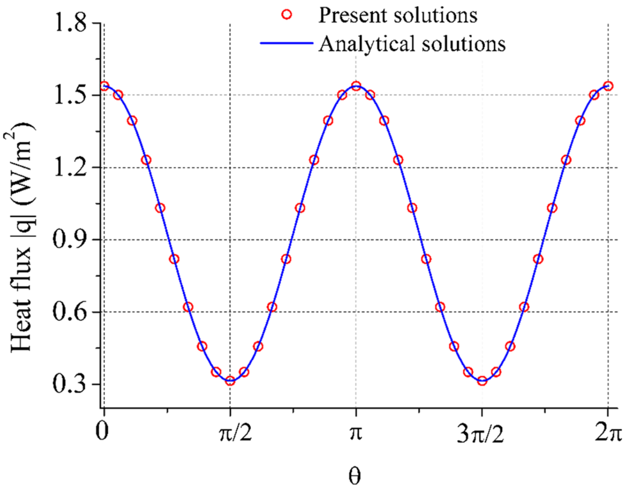

Fig. 7 The numerical results of heat flux q at the points along S1

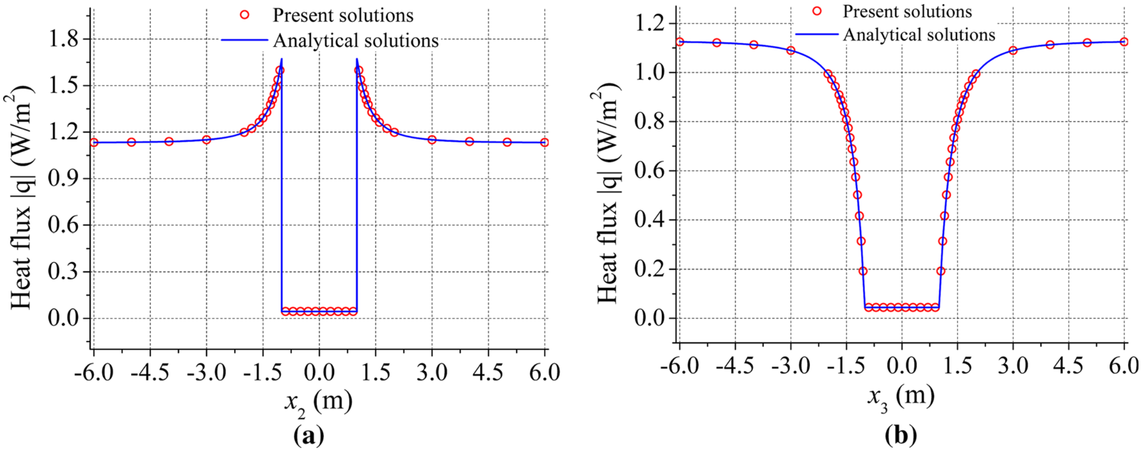

Fig. 6 Comparison of heat flux q distribution for the present results and the analysis solutions for the case $k_I < k_M$: **a** along x_2 axis and **b** along x_3 axis

Fig. 8 The heat flux q distribution at $x_2 - x_3$ surface for the case $k_I < k_M$: **a** present results, **b** analytical results

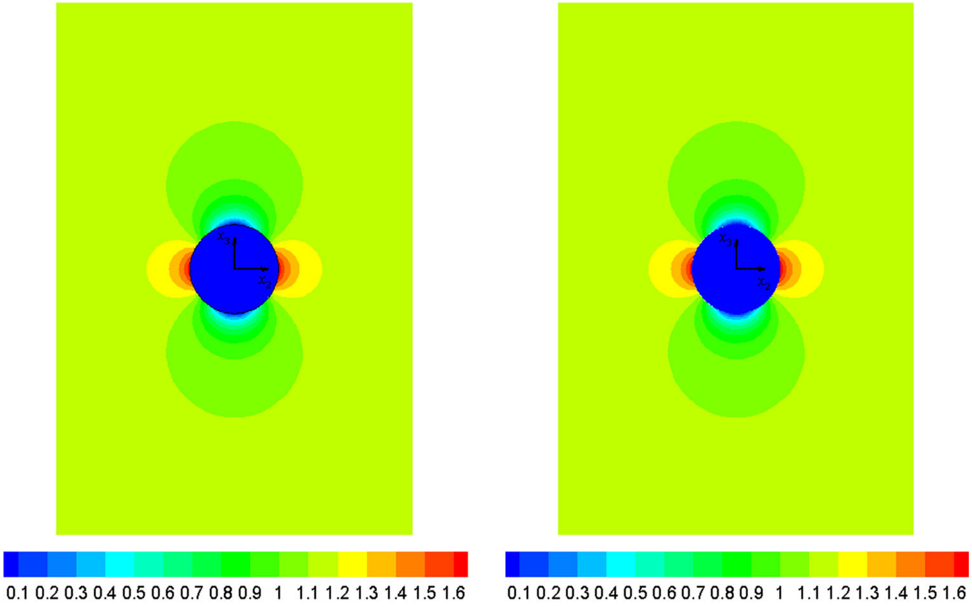

(a) **(b)**

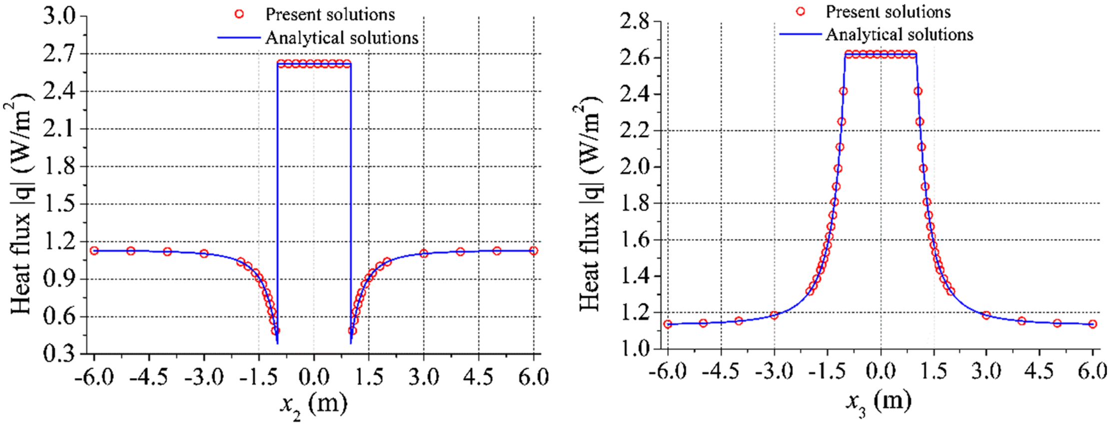

(a) **(b)**

Fig. 9 Comparison of heat flux q distribution for the present results and the analytical solutions for the case $k_I > k_M$: **a** along x_2 axis, **b** along x_3 axis

convergent to constant loading q_3 at the distance of four or five times of the inclusion's radius ($4a \sim 5a$), namely, the effect of inclusion will disappear when the distance between the computed points and the center of the inclusion is over $5a$. The conclusion will be of great importance for the computation of infinite problems using FEM and some commercial software.

Figure 7 shows the numerical results of heat flux when the computed points are moving along the curve (S1), i.e. S1: $x_1 = 0,\ \ x_2 = a\cos\theta,\ \ x_3 = a\sin\theta\ (a = 1.1)$, and the exact solutions are given as comparison. From Fig. 7, we can clearly see that the current solutions are in good agreement with the exact results.

In Fig. 8a, the present numerical result of flux q for this problem is shown. For comparison, the contour plot of the analytic flux is also given in Fig. 8b. From Fig. 8a, b, it can be seen that the computational results are in good agreement with the analytic results. Figure 8a, b also tell us that the values of heat flux along x_2 axis are much bigger than those along x_3 axis. However, the influence range of inclusion on heat flux along x_3 axis is much larger than that along x_2 axis.

5.2 A single spherical inclusion embedded in an infinite matrix for the case ($k_I > k_M$)

To study the effect of thermal conductivity of the inclusion on the disturbance of heat flux, another single spherical inclusion composed of quartz is used for discussion and its geometry is shown in Figs. 4 and 5. The thermal conductivity of the inclusion is $k_I = 7.69$ W/m K [54]. Different from the

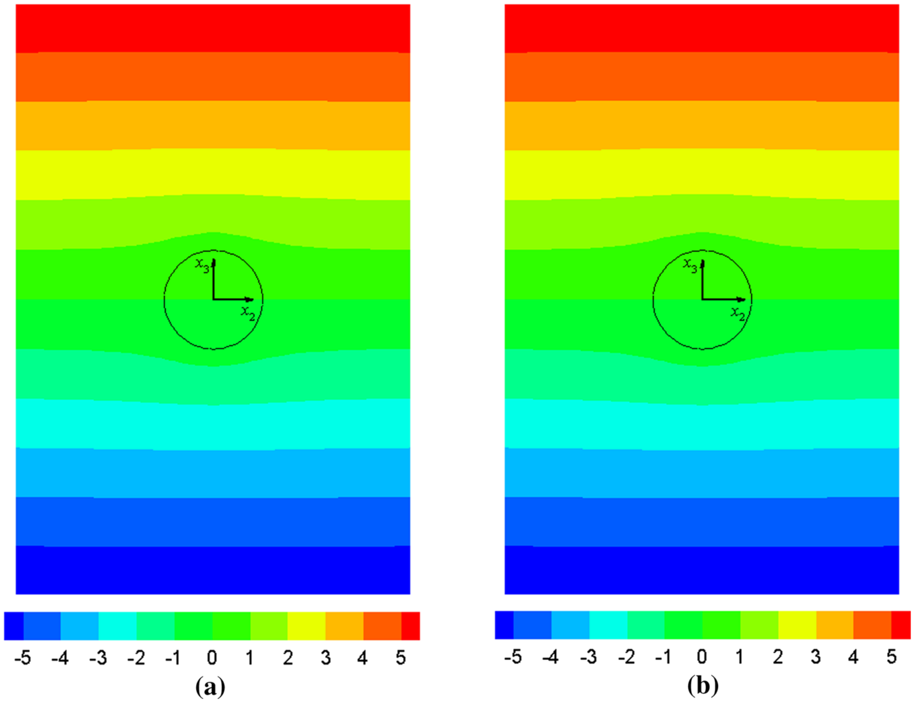

Fig. 10 The temperature T distribution at $x_2 - x_3$ surface for the case $k_I > k_M$: **a** present results, **b** analytical results

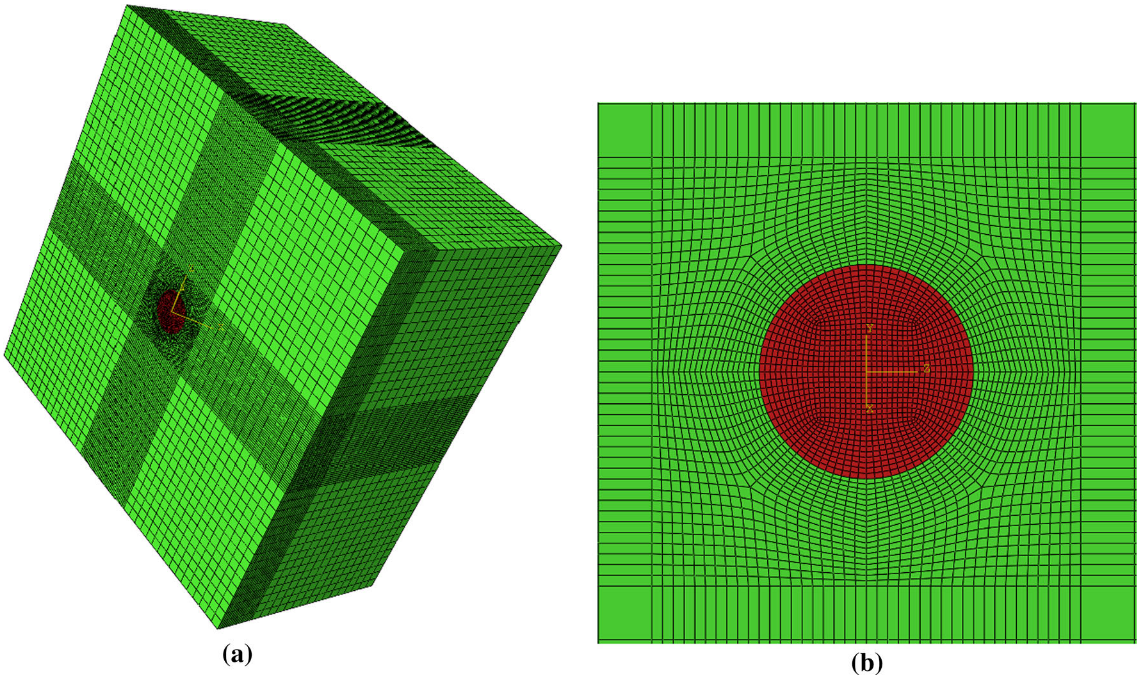

Fig. 11 FE model for an inclusion embedded in an infinite matrix: **a** mesh of the model, and **b** mesh near the inclusion

case in example 5.1, the thermal conductivity of the inclusion is bigger than that of the matrix ($k_M = 1.13$ W/m K).

Figure 9 compares the heat flux distribution along the x_2 and x_3 for the present results and analytical solutions. From Fig. 9, it can be seen that the magnitude of heat flux field keeps constant among the inclusion domain, but greater than the surrounding values. Along the axis x_2 the heat flux reaches its minimum at the outer surface of the particle and then gradually increases to q_3 in the far field of the matrix material. Along the axis x_3, some similar conclusions as example 5.1 can be obtained: the distribution of heat flux field is nearly linear in the inclusion domain and continuous even across the interface.

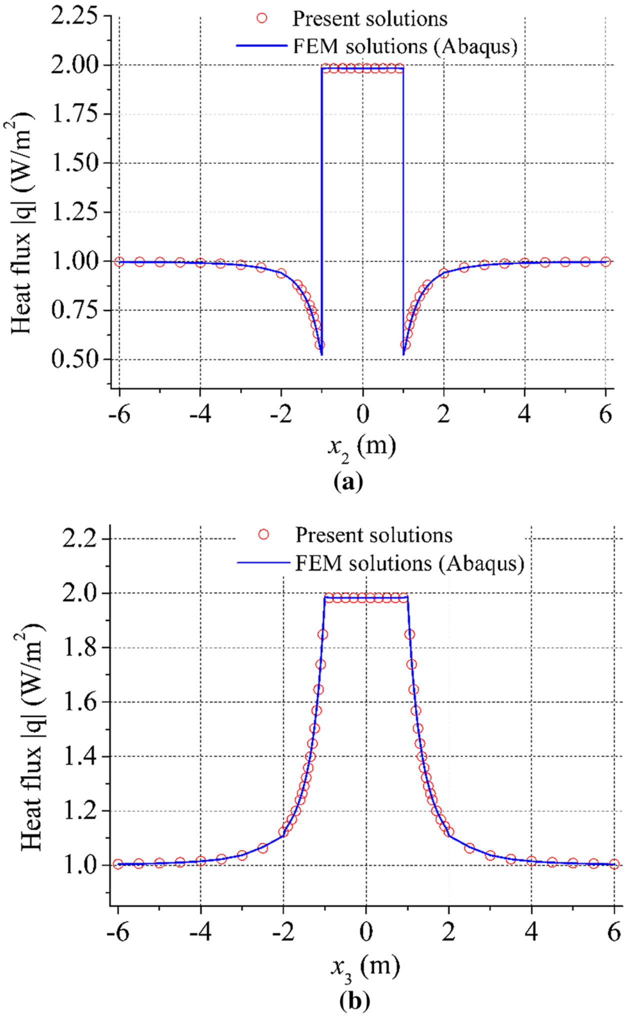

(a)

(b)

Fig. 12 Comparison of heat flux q distribution for the present results and the reference (FEM) solutions: **a** along x_3 axis, **b** along x_3 axis

To further study the influence of inclusion thermal conductivity on temperature, Fig. 10a, b respectively give the contour plots of temperature distribution obtained by the present and analytical methods. As shown in Fig. 10, there is an excellent agreement between the contours from the present technique and analytical method.

5.3 An orthotropic spherical inclusion embedded in an infinite matrix

The previous examples have investigated the accuracy of the proposed algorithms with respect to the heat conduction of an isotropic inclusion embedded in an infinite borosilicate glass. Here, the focus is to investigate the effect of orthotropic inclusion on the distribution of heat flux. The thermal conductivity of the inclusion is taken as [55]

$$k_I = \begin{bmatrix} 6.1135 & 0 & 0 \\ 0 & 0.4829 & 0 \\ 0 & 0 & 4.4036 \end{bmatrix} \quad (43)$$

Similar to the above example, the spherical orthotropic inclusion ($0 \le r < a$, $a = 1$) is embedded in an infinite borosilicate glass subject to a remote uniform flux along x_3.

Here, a finite element model is constructed with the FEM software Abaqus to offer a reference solution. Based on the geometry, an axisymmetric problem is considered as shown in Fig. 11a. The size of the matrix is $2\beta \times 2\beta \times \beta$, and the radius of the inclusion is a. According to the above conclusions, the matrix size $\beta = 10a$ is used, which was found to provide a convergent solution for the local heat flux field in this problem. Structured hexahedral elements are employed, where the edge length of the elements in the inclusion is 0.05, whereas those for the matrix are mostly 0.5. However, in the neighborhood of the inclusion, a transition zone is meshed with the same element size as the inclusion area. Figure 11a, b illustrates the finite element mesh. The mesh consists of 210,624 elements and 221,993 nodes.

Figure 12a, b shows some results at points along the axis x_2 and x_3 from present method and FEM (Abaqus), respectively, for heat fluxes. One can find that the results are in good agreement with the FEM solutions for the two directions. Since a remote uniform flux along x_3 is applied to the model, the curve of heat flux disturbed by the orthotropic inclusion looks very similar to the results shown in Fig. 9.

Fig. 13 Isogeometric model of the prolate spherical inclusion and its control points

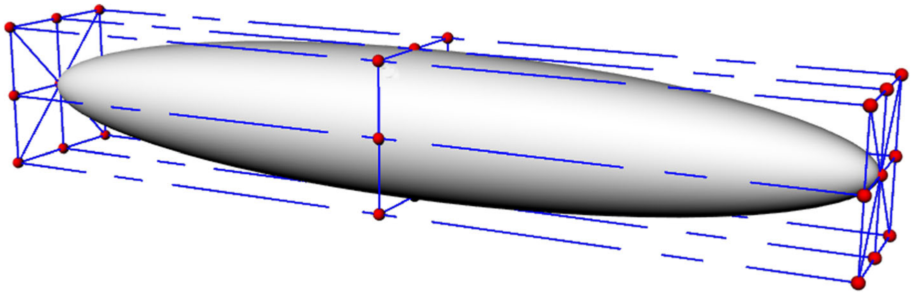

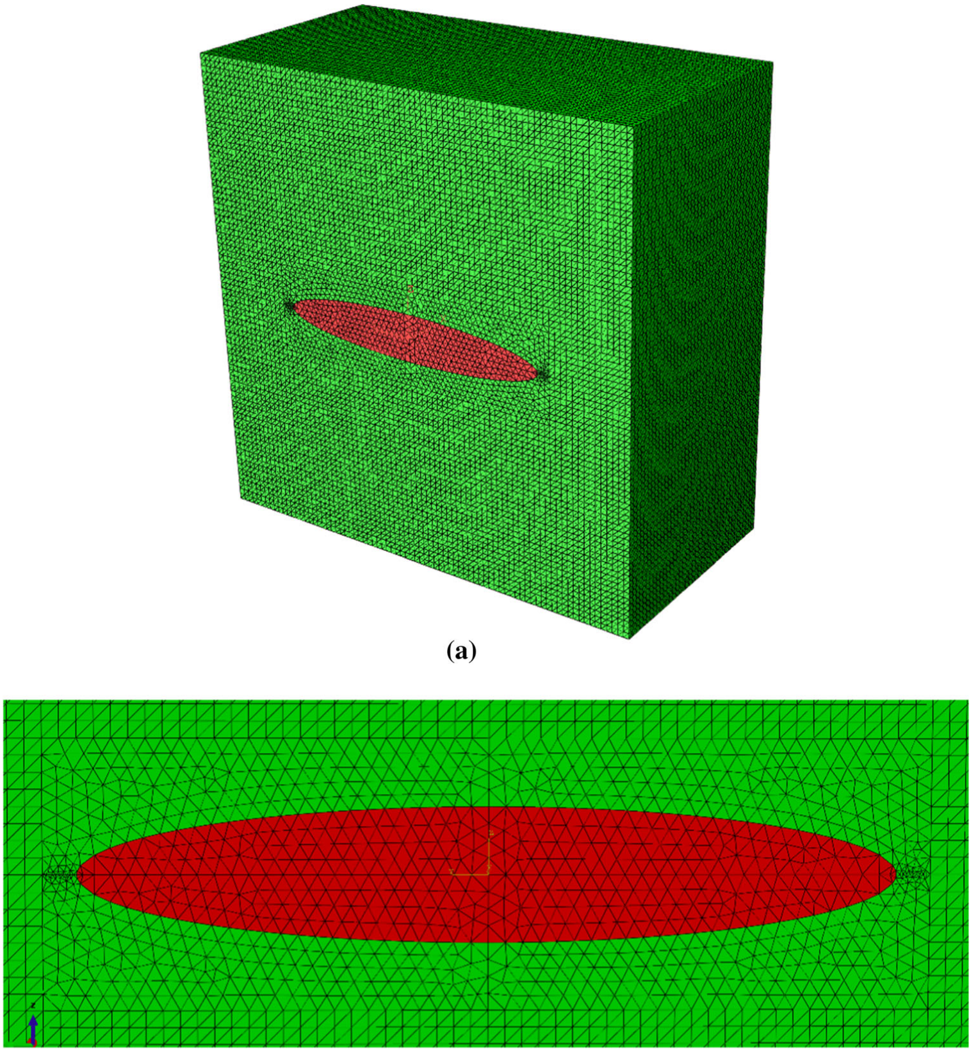
(a)

(b)

Fig. 14 FE model for a prolate spherical inclusion embedded in an infinite matrix: **a** mesh of the model, and **b** mesh near the inclusion

5.4 A prolate spherical inclusion embedded in an infinite matrix

In the mechanical industry, prolate spherical inclusion has been one of the most critical models and has been studied widely in a variety of problems. The analysis of heat conduction for prolate spherical inclusion is of great importance in many practical transmission systems. In the fourth example, a single prolate spherical air void ($k_I = 0.03$ W/m K) embedded in an infinite isotropic borosilicate glass ($k_M = 1.13$ W/m K) which is subjected to heat flux field with $q_3 = 1$, is investigated. Here, we will consider the influence of inclusion shape on the distribution of heat flux. Suppose the geometry of the ellipsoidal particle is

$$\frac{x_1^2}{a^2} + \frac{x_2^2}{b^2} + \frac{x_3^2}{c^2} = 1 \tag{44}$$

where $a = c = 1$ and b varies from 2 to 6. In the numerical computation, the geometry of the inclusion is also described by bivariate NURBS basis functions and control points of the inclusion ($a = c = 1$, $b = 6$) are shown in Fig. 13.

Finite element models are constructed with the FEM software Abaqus to offer reference solutions. Tetrahedral elements are employed, where the edge length of the elements in the inclusion and the matrix are mostly 0.25. However, in the neighborhood of the inclusion, a transition zone is meshed with the 0.05 element size. Figure 14a, b illustrates the finite element mesh for $b = 6$. As shown in Fig. 14a, b, the tip of the ellipsoid is locally refined to obtain more accurate results for the data in Fig. 15a. The mesh for the case $b = 6$ consists of 1,273,637 elements and 1,746,517 nodes. The mesh for $b = 2 (b = 4)$ consists of 1,319,488 (1,321,819) elements and 1,807,529 (1,810,414) nodes.

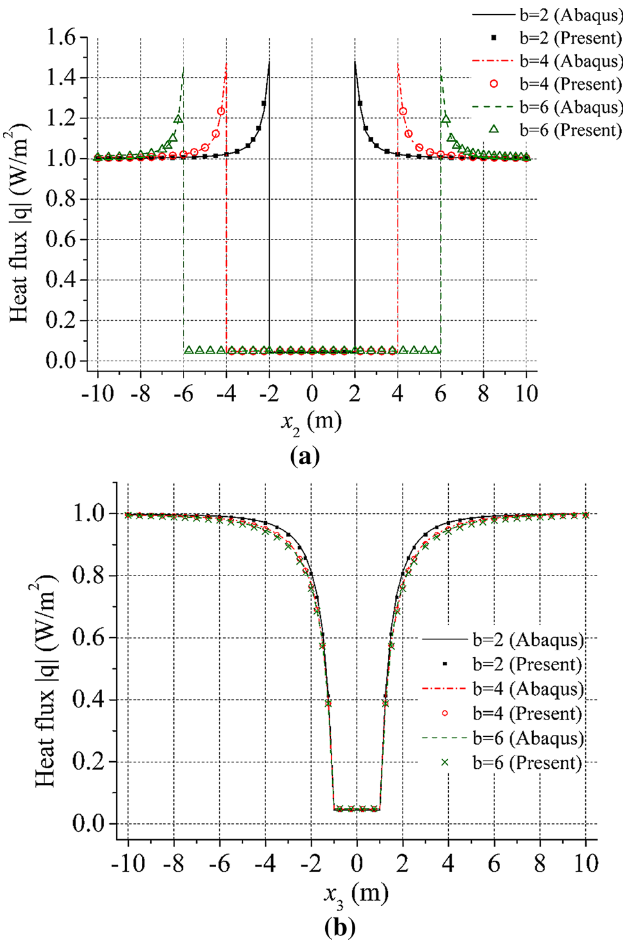

Fig. 15 Comparison of heat flux q distribution for the present results and the reference solutions: **a** along x_2 axis and **b** along x_3 axis

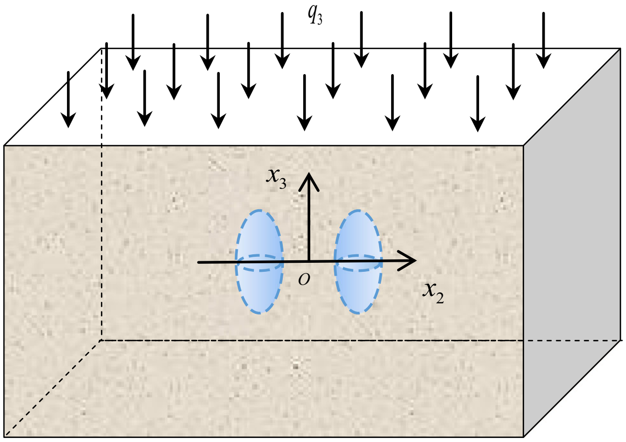

Fig. 16 The model of matrix and two prolate spherical inclusions

Figure 15a, b compares the heat flux distribution along the axes x_2 and x_3 for the present numerical results and FEM solutions when b varies from 2 to 6. From Fig. 15a, b, one can find that the magnitude of heat flux field is nearly uniform in the particle domain. Along x_2 axis, the heat flux is highly discontinuous across the contact surface of inclusion and matrix and the heat flux reaches the maximum at the interface. With the increase of b, the heat flux of the contact surface is smaller, but gradually decreases and converges to $1.0\mathrm{W/m}^2$, which is the uniform far field loading. As shown in Fig. 15b, when b is increasing, the heat flux near the inclusion has a decreasing trend. However, when b is greater than 4, the heat flux nearly keeps stable.

5.5 Two prolate spherical inclusions embedded in an infinite matrix

As shown in Fig. 16, two prolate spherical air void inclusions ($k_I = 0.03$ W/m K) are embedded in an infinite isotropic borosilicate glass ($k_M = 1.13$ W/m K) which is subjected to heat flux field with $q_3 = 1$. In the numerical computation, the geometry of the inclusions are also depicted by bivariate NURBS basis functions. The control points of the inclusions are shown in Fig. 17a. Cutting surface of the model is given in Fig. 17b, in which the hollow circles denote the collocation points for radial basis function method and red points represent the control points.

Here, a finite element model is constructed with the FEM software Abaqus to offer a reference solution. Tetrahedral

Fig. 17 Isogeometric model of the two inclusions. **a** The control points of the inclusions, **b** cutting surface of the model

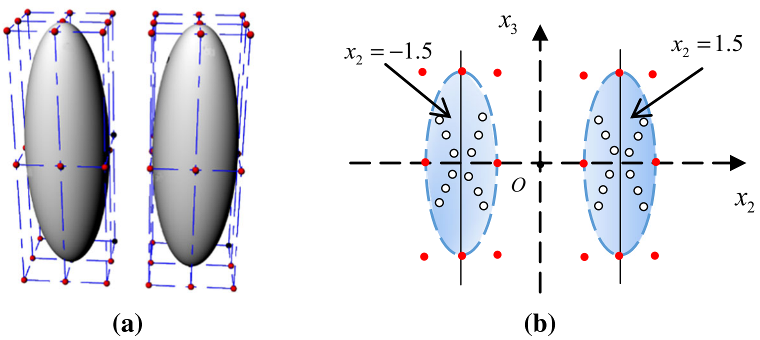

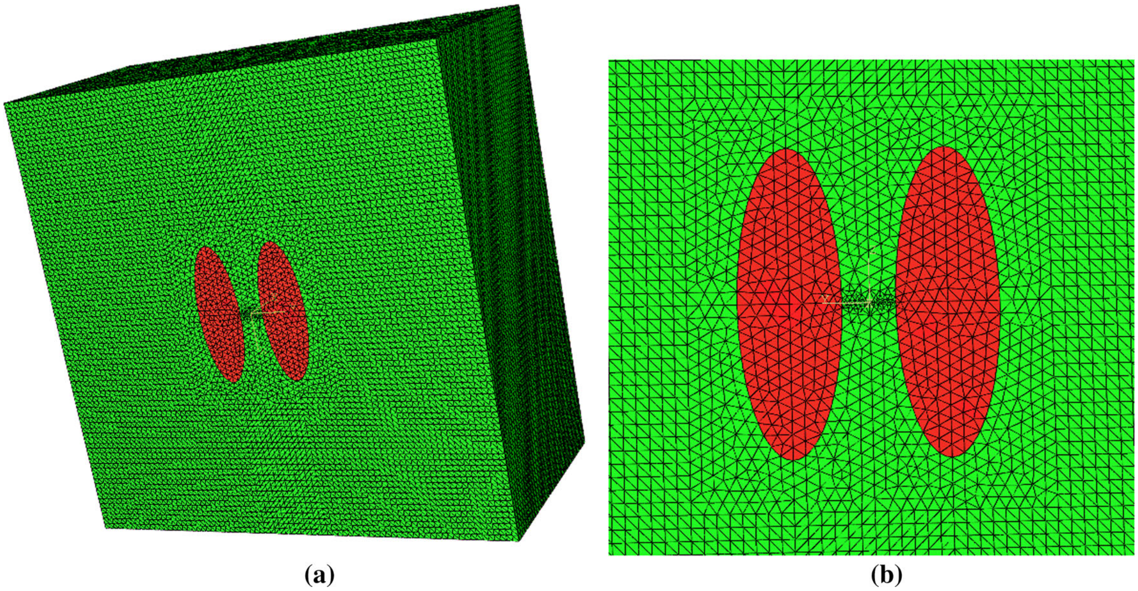

Fig. 18 FE model for two spheroid inclusions embedded in an infinite matrix: **a** mesh of the model, and **b** FE mesh near the inclusions

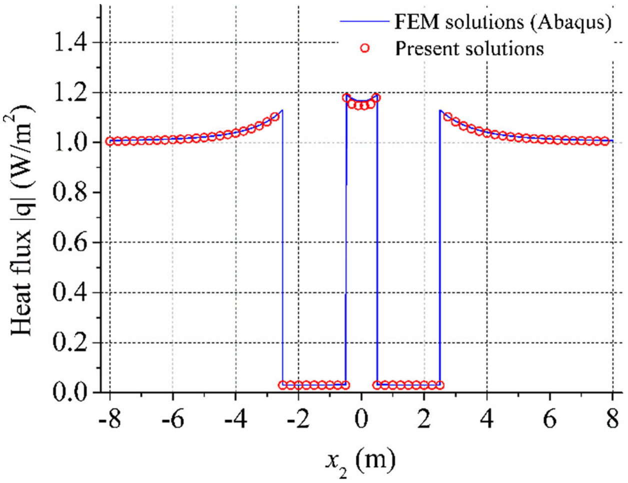

Fig. 19 Comparison of heat flux q distribution along x_2 obtained by using present method and FEM

elements are employed, where the edge length of the elements in the inclusion and the matrix are mostly 0.25, whereas the mesh size between the two inclusions is 0.05. Figure 18a, b illustrates the finite element mesh. As shown in Fig. 18a, b, the middle part of the two inclusions along x_2 axis is locally refined, which makes the FEM results more accurate in Fig. 19. The mesh consists of 1,402,552 elements and 1,917,907 nodes.

The comparison of heat flux distribution along x_2 obtained by using present method and FEM are shown in Fig. 19, in which the results obtained by the two methods are excellently consistent with each other. And the numerical accuracy of proposed technique is also tested by evaluating the heat flux distribution along the lines $x_2 = \pm 1.5$ indicated in Fig. 17b. Also, good agreement is shown in Fig. 20a, b. Apparently, owing to the symmetry of the two inclusions in terms of the x_3 axis, the curves of heat flux along the two lines are similar.

Figure 21a, b shows the heat flux contours computed by the present method and FEM, from which the influence of two prolate spherical air void inclusions on the whole field can be seen clearly. Figure 21a, b also imply that the accuracy of the present method is satisfactory in the whole field of the problem.

5.6 100 spherical inclusions embedded in an infinite matrix

As shown in Eqs. (20) and (21), the present method can handle larger scale 3D problems. In this part, a model with 100 unit spherical inclusions is considered. Figure 22 gives the inclusion distribution in the computational model. The heat conductivities of the inclusions and matrix are taken as $k_I = 0.5$ W/m K and $k_M = 1.0$W/m K, respectively. Heat flux q along the negative direction of the x_3 axis ($q_3 = 1.0\text{W/m}^2$) is applied on the matrix. Figure 23 shows the flux distribution with matrix and inclusions. The influence of inclusions on heat fluxes disappear (heat flux equal to q_3) when the points are far away from the inclusions. And due to the large distance ($a = 4$) between inclusions and small heat conductivity, the flux inside the inclusion keeps same color (seems no effect on each inclusion).

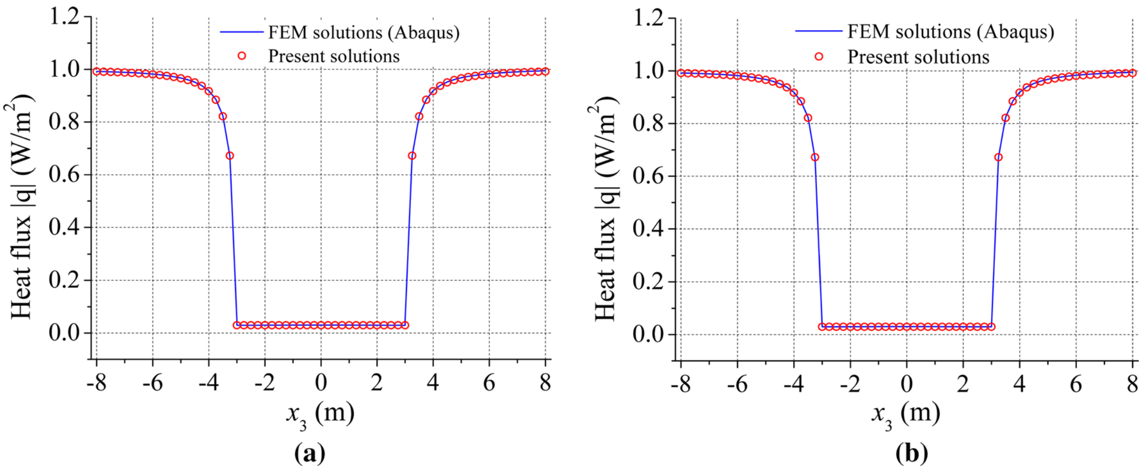

(a) (b)

Fig. 20 Heat flux q distribution along the lines: **a** $x_2 = 1.5$ and **b** $x_2 = -1.5$

Fig. 21 Heat flux q contours computed by the present method and FEM. **a** Contour of present results, **b** contour of FEM results

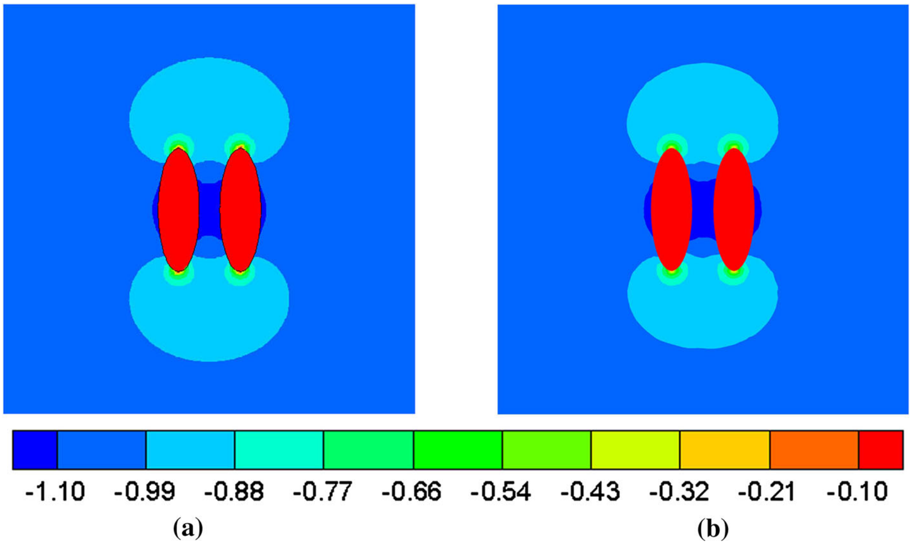

(a) (b)

To study the interaction between inclusions and the heat flux distribution inside the inclusions, distances a in Fig. 22c are reduced to 3. The heat conductivities of the inclusions k_I are increase to 10 W/m K and heat conductivities of the matrix k_M keeps 1.0W/m K. Figure 24 shows the heat flux distribution within the inclusions and the matrix. We can see that the heat flux distribution around the inclusions is very similar to the heat flux distribution in Fig. 23. However, the heat flux distribution inside the inclusion is very different from that in Fig. 23. From Fig. 24 we can clearly see the heat flux distribution inside the inclusions.

6 Conclusions

In this paper, a new regularized interface-domain integral equation is firstly developed for solving 3D heat conduction problems with inclusions. The proposed formulations only contain the fundamental solution of isotropic matrix so that the fundamental solution of non-homogeneous inclusion is avoided. Then, radial integration method is used to deal with the domain integral due to the contrast of conductivities between the inclusion and the matrix, and the radial basis functions are employed to approximate the unknowns appearing in the domain integral. Finally, the domain integrals appearing in the regularized interface-domain integral equation is transformed to interface integrals using the radial integration method. As a result, finite elements are not

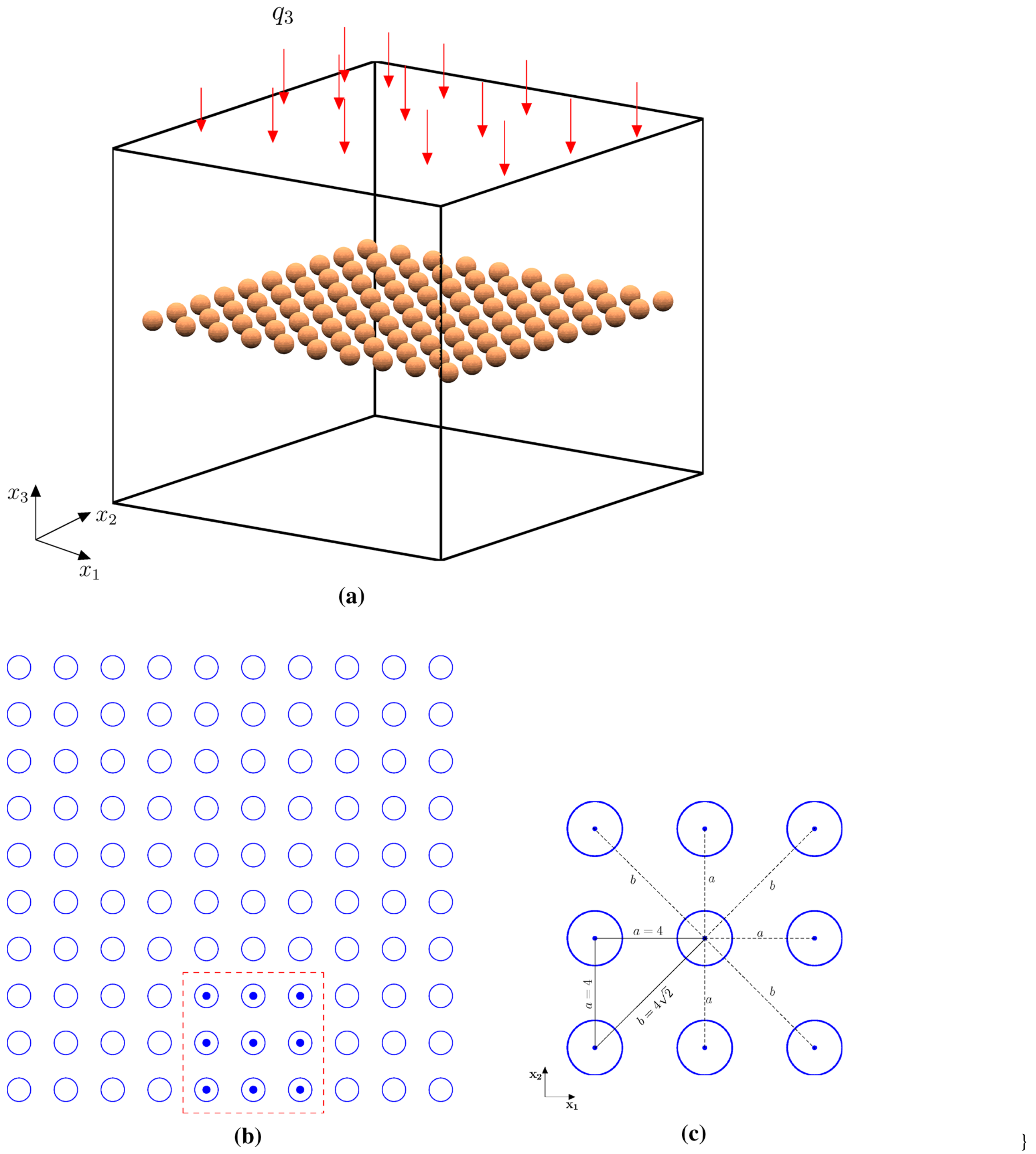

Fig. 22 Position relationship of inclusions in the computational model. **a** 100 inclusions embedded in an infinite domain model, **b** 100 inclusions cut by $x_1 - x_2$ plane, **c** relationship between the inclusions in the red dashed box

required in the numerical implementation of the domain integral equation for inclusion problems any more.

In the numerical computation, the geometry of the inclusions is depicted by bivariate NURBS basis functions. Compared with traditional BEM, the inclusions for analysis in the proposed method has exact geometrical representation no matter how coarse the discretization of the studied particles are. That is to say, the method ensures that no geometrical errors appear in the analysis process. This is a distinct advantage over traditional BEM, in which the geometrical errors will greatly influence the accuracy of the numerical result, especially for complex models.

To offer a reference solution, several finite element models are constructed by means of the FEM software Abaqus. In all the examples, we compared the present results with those obtained by the analytical method or FEM. The given numerical examples have demonstrated the correctness and effectiveness of the developed method.

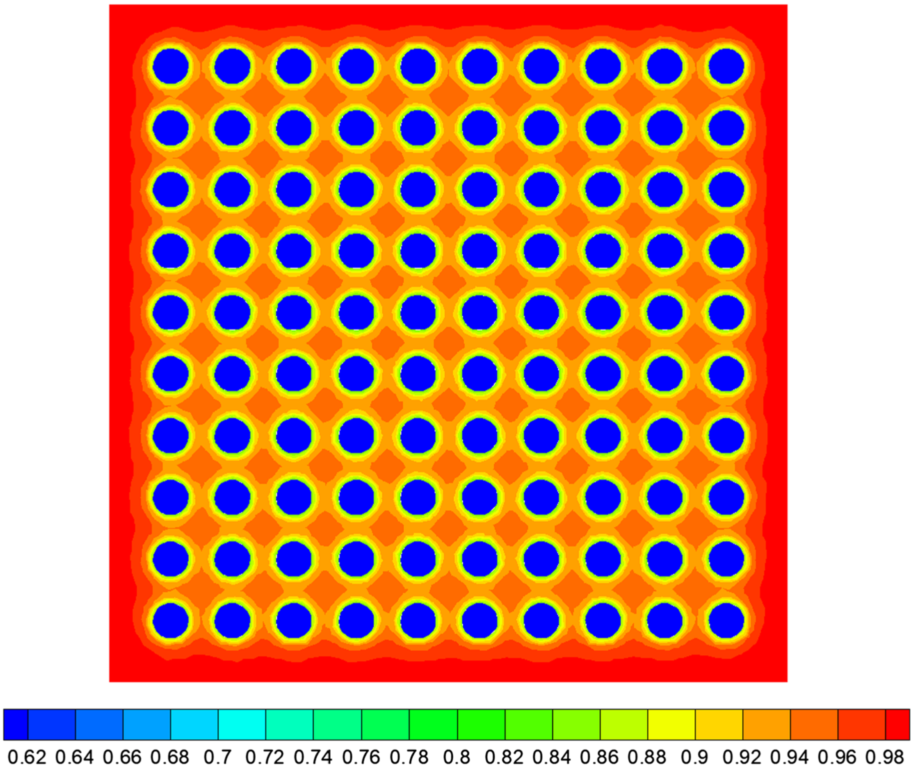

Fig. 23 Heat flux q distribution within the inclusions and the matrix at the $x_1 - x_2$ surface for distance $a = 4$

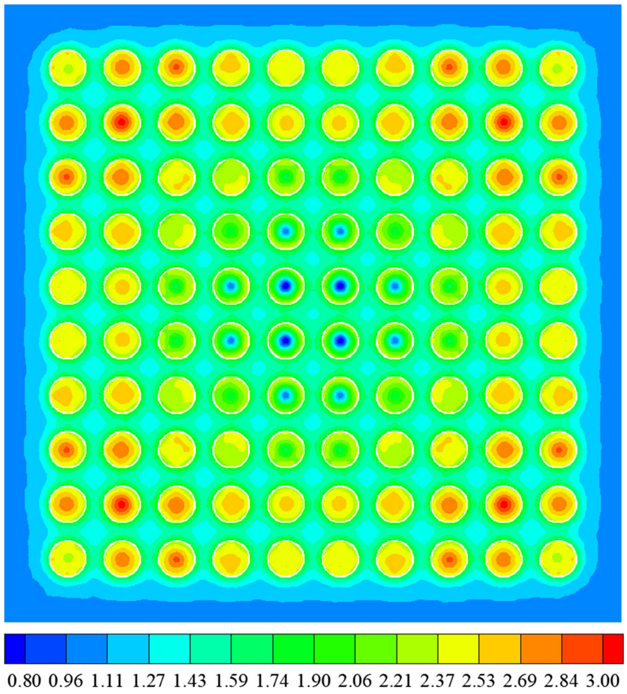

Fig. 24 Heat flux q distribution within the inclusions and the matrix at $x_1 - x_2$ surface when distance $a = 3$

Acknowledgements The research is supported by the National Natural Science Foundation of China (11672038, 11272054). Y.P. Gong is also supported by the Graduate Technological Innovation Project of Beijing Institute of Technology (2017CX10033).

References

1. Eshelby JG (1957) The determination of the elastic field of an ellipsoidal inclusion, and related problems. Proc R Soc Lond A 241:376–396
2. Muskhelishvili NI (1953) Some basic problems of mathematical theory of elasticity. Noordhorff, Groningen
3. Hwu C, Yen WJ (1993) On the anisotropic elastic inclusions in plane elastostatics. J Appl Mech 60:626–632
4. Eshelby JG (1959) The elastic field outside an ellipsoidal inclusion. Proc R Soc Lond A 252:561–659
5. Zienkiewicz OC, Taylor RL (2000) The finite element method, 5th edn. Butterworth-Heinemann, London
6. Ghosh S, Mukhopadhyay SN (1993) Amaterial based finite element analysis of heterogeneous media involving Dirichlet tessellations. Comput Methods Appl Mech Eng 104:211–247
7. Nakamura T, Suresh S (1993) Effects of thermal residual stresses and fiber packing on deformation of metal-matrix composites. Acta Metall Mater 41:1665–1681
8. Thomson RD, Hancock JW (1984) Local stress and strain fields near a spherical elastic inclusion in a plastically deforming matrix. Int J Fract 24:209–228
9. Zhang J, Katsube N (1995) A hybrid finite element method for heterogeneous materials with randomly dispersed elastic inclusions. Finite Elem Anal Des 19:45–55
10. Beck JV (2010) Heat conduction using Green's functions. Hemisphere Pub. Corp., Washington
11. Ozisik MN (1993) Heat conduction, 2nd edn. Wiley, New York
12. Hiroshi H, Minoru T (1986) Equivalent inclusion method for steady state heat conduction in composites. Int J Eng Sci 24(7):1159–1172
13. Brebbia CA, Dominguez J (1989) Boundary elements: an introduction course. Computational Mechanics Publications/McGraw-Hill, New York

14. Bonnet M (1999) Boundary integral equation methods for solids and fluids. Wiley, New York
15. Cruse TA (1988) Boundary element analysis in computational fracture mechanics. Kluwer Academic Publishers, Dordrecht
16. Rizzo FJ (1967) An integral equation approach to boundary value problems of classical elastostatics. Q Appl Math 25:83–95
17. Dong CY, Lo SH, Cheung YK (2003) Interaction between coated inclusions and cracks in an infinite isotropic elastic medium. Eng Anal Bound Elem 27:871–884
18. Dong CY (2015) An interface integral formulation of heat energy calculation of steady state heat conduction in heterogeneous media. Int J Heat Mass Transf 90:314–322
19. Dong CY (2015) Boundary integral equation formulations for steady state thermal conduction and their applications in heterogeneities. Eng Anal Bound Elem 54:60–67
20. Dong CY, Lo SH, Cheung YK (2004) Numerical solution for elastic inclusion problems by domain integral equation with integration by means of radial basis functions. Eng Anal Bound Elem 28:623–632
21. Zhang YM, Sladek V, Sladek J, Liu ZY (2012) A new boundary integral equation formulation for plane orthotropic elastic media. Appl Math Model 36:4862–4875
22. Zhang YM, Liu ZY, Gao XW, Sladek V, Sladek J (2014) A novel boundary element approach for solving the 2D elasticity problems. Appl Math Comput 232:568–580
23. Qu WZ, Zhang YM, Gu Y, Wang FJ (2017) Three-dimensional thermal stress analysis using the indirect BEM in conjunction with the radial integration method. Adv Eng Softw 112:147–153
24. Wilson RB, Cruse TA (1978) Efficient implementation of anisotropic three dimensional boundary-integral equation stress analysis. Int J Numer Meth Eng 12:1383–1397
25. Lee J, Choi S, Mal A (2001) Stress analysis of an unbounded elastic solid with orthotropic inclusions and voids using a new integral equation technique. Int J Solids Struct 38:2789–2802
26. Buryachenko VA, Bechel VT (2000) A series solution of the volume integral equation for multiple inclusion interaction problems. Compos Sci Technol 60:2465–2469
27. Dong CY, Lo SH, Cheung YK (2002) Application of boundary-domain integral equation in elastic inclusion problems. Eng Anal Bound Elem 26:471–477
28. Gao XW, Davies TG (2002) Boundary element programming in mechanics. Cambridge University Press, Cambridge
29. Nardini D, Brebbia CA (1982) A new approach for free vibration analysis using boundary elements. In: Brebbia CA (ed) Boundary element methods in engineering. Springer, Berlin, pp 312–326
30. Nowak AJ, Brebbia CA (1989) The multiple-reciprocity method. A new approach for transforming B.E.M. domain integrals to the boundary. Eng Anal Bound Elem 6:164–168
31. Takhteyev V, Brebbia CA (1990) Analytical integrations in boundary elements. Eng Anal Bound Elem 7:95–100
32. Gao XW (2002) A boundary element method without internal cells for two-dimensional and three-dimensional elastoplastic problems. J Appl Mech Trans ASME 69:154–160
33. Gao XW (2002) The radial integration method for evaluation of domain integrals with boundary-only discretization. Eng Anal Bound Elem 26:905–916
34. Yang K, Wang J, Du JM, Peng HF, Gao XW (2017) Radial integration boundary element method for nonlinear heat conduction problems with temperature-dependent conductivity. Int J Heat Mass Transf 104:1145–1151
35. Yang K, Peng HF, Wang J, Xing CH, Gao XW (2017) Radial integration BEM for solving transient nonlinear heat conduction with temperature-dependent conductivity. Int J Heat Mass Transf 108:1551–1559
36. Hughes TJ, Cottrell JA, Bazilevs Y (2005) Isogeometric analysis: CAD, finite elements, NURBS, exact geometry and mesh refinement. Comput Methods Appl Mech Eng 194:4135–4195
37. Farin G, Hoschek J, Kim M-S (eds) (2002) Handbook of computer aided geometric design. Elsevier, Amsterdam
38. Verhoosel CV, Scott MA, Hughes TJ, De Borst R (2011) An isogeometric analysis approach to gradient damage models. Int J Numer Methods Eng 86:115–134
39. Zhang H, Wang D (2015) An isogeometric enriched quasi-convex meshfree formulation with application to material interface modeling. Eng Anal Bound Elem 60:37–50
40. Tang S, Kopacz AM, O'Keeffe SC, Olson GB, Liu WK (2013) Concurrent multiresolution finite element: formulation and algorithmic aspects. Comput Mech 52(6):1265–1279
41. Liu Z, Fleming M, Liu WK (2018) Microstructural material database for self-consistent clustering analysis of elastoplastic strain softening materials. Comput Methods Appl Mech Eng 330:547–577
42. Sakuma T, Yasuda Y (2002) Fast multipole boundary element method for large-scale steady-state sound field analysis. Part I: setup and validation. Acta Acust United Acust 88(4):513–525
43. Liu Y, Nishimura N, Otani Y (2005) Large-scale modeling of carbon-nanotube composites by a fast multipole boundary element method. Comput Mater Sci 34(2):173–187
44. Dong C, Bonnet M (2002) An integral formulation for steady state elastoplastic contact over a coated half-plane. Comput Mech 28:105–121
45. Wang L, Zhou X, Wei X (2008) Heat conduction: mathematical models and analytical solutions. Springer, Berlin
46. Simpson RN, Bordas SPA, Trevelyan J, Rabczuk T (2012) A two-dimensional isogeometric boundary element method for elastostatic analysis. Comput Methods Appl Mech Eng 209–212:87–100
47. Gu JL, Zhang JM, Li GY (2012) Isogeometric analysis in BIE for 3-D potential problem. Eng Anal Bound Elem 36:858–865
48. Simpson RN, Bordas SPA, Lian H, Trevelyan J (2013) An isogeometric boundary element method for elastostatic analysis: 2D implementation aspects. Comput Struct 118:2–12
49. Gong YP, Dong CY, Qin XC (2017) An isogeometric boundary element method for three dimensional potential problems. J Comput Appl Math 313:454–468
50. Gong YP, Dong CY (2017) An isogeometric boundary element method using adaptive integral method for 3D potential problems. J Comput Appl Math 319:141–158
51. Yin HM, Paulino GH, Buttlar WG, Sun LZ (2008) Heat flux field for one spherical inhomogeneity embedded in a functionally graded material matrix. Int J Heat Mass Transf 51:3018–3024
52. Hammerschmidt U, Abid M (2015) The thermal conductivity of glass-sieves: I. Liquid saturated frits. Int J Therm Sci 96:119–127
53. Carslaw HS, Jaeger JC (1959) Conduction of heat in solid. Oxford University Press, Oxford
54. Abid M, Hammerschmidt U, Köhler J (2014) Thermophysical properties of a fluid-saturated sandstone. Int J Therm Sci 76(2):43–50
55. Powers JM (2013) On the necessity of positive semi-definite conductivity and Onsager reciprocity in modeling heat conduction in anisotropic media. J Heat Transf 126(5):767–776